Lecture 5

Scanning Tunneling and Atomic Force Microscopy

The tunneling current, $J_t = CV\exp[-A\sqrt{E_w}\delta_z]$

C and A are constants, V is the voltage applied to the tip.
Δz is the probe distance, of the order of 10 A. E_w is the work function.

Tunneling current varies exponentially with distance and is detectable only within a few Angstroms.

For a rectangular barrier, the one dimensional wave equation is,
$\Psi = e^{\pm kz}$ where $k = 2m(V_B\text{-}E)/\hbar^2$

V_B may be constant across the gap, but need not be. For states at Fermi level, V_B-E is the work function.

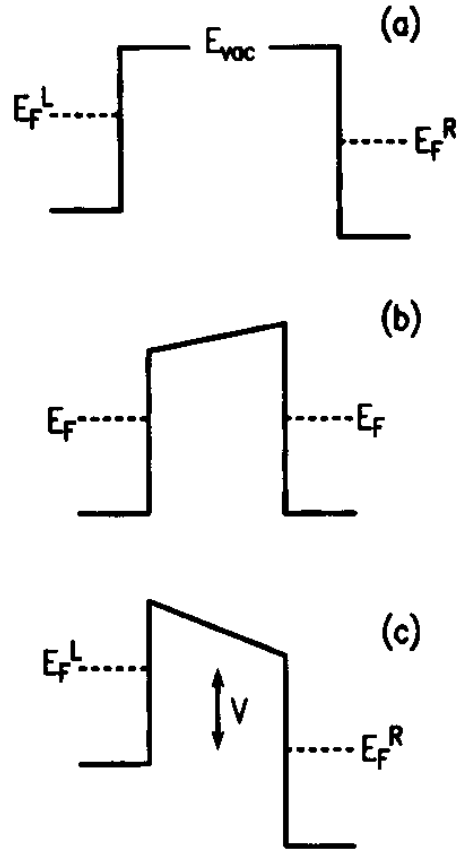

FIG. 1. Schematic of potential barrier between electrodes for vacuum tunneling. (a) Two non-interacting metal electrodes, separated by vacuum. The Fermi levels E_F of the two materials differ by an amount equal to the work function difference. (E_F^L and E_F^R denote the Fermi levels of the left and right electrode respectively, in the cases (a) and (c) where the two are not in equilibrium.) (b) The two electrodes are allowed to come into electrical equilibrium, so that there is a unique common Fermi level. The difference in work functions is now manifested as an electric field in the vacuum region. (c) A voltage is applied. There is a voltage drop V across the gap, i.e., the Fermi levels differ by eV. The field in the barrier includes contributions from both the applied voltage and the work function difference. The arrows indicate the range of energy over which tunneling can occur. At higher energies, there are no electrons to tunnel, while at lower energies, there are no empty states to tunnel into.

The transmission probability or the tunneling current varies exponentially with the
Distance. $I \alpha e^{-2kd}$

Common work functions are 4-5 eV and therefore, 2k is of the order of $2A^{-1}$

Tunneling current drops by an order of magnitude for every 1A of vacuum between electrodes. Thus, this current can be observed in practice only at small Separations.

To keep the current stable requires precise control of distances.

The first experimental observation of controlled vacuum tunneling was by Bining et. al. in 1982. They used a piezo electric device to control the distance.

Earlier studies of tunneling were using a static barrier, such as an oxide sandwiched between electrodes.

Tunneling schematic

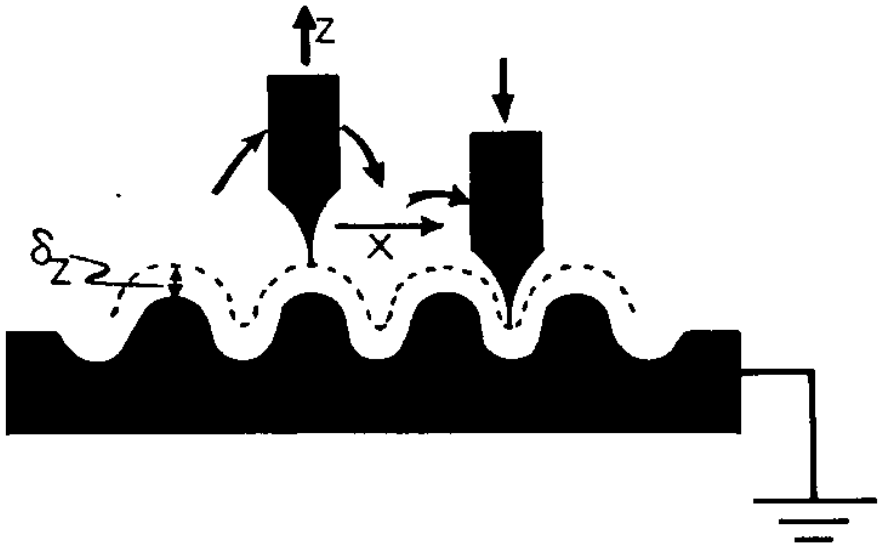

FIG. 2.31 *A field-emission end form is moved along a grating surface so that electron tunneling current remains constant, tracing the profile of the hills and valleys of the grating.*

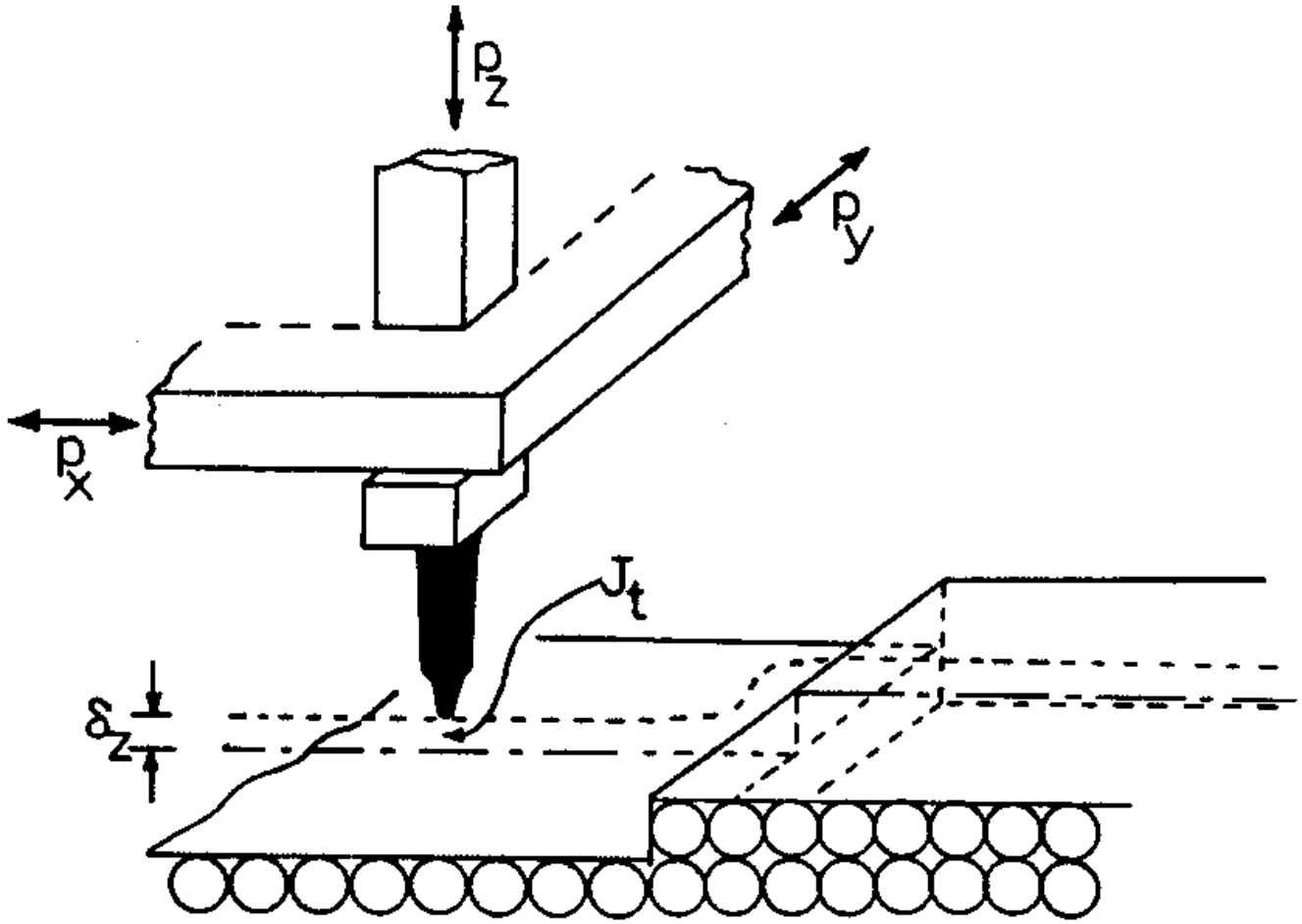

(a) Sharp metal tip scans the surface. The piezoelectric scanners position the tip accurately over the sample. The tip scans in the x and y directions, the position of z is adjusted to make by the feedback circuit to make the tunneling current constant. The path of the tip reproduces the shape of the surface. This is the common constant current mode of STM operation. There is also a constant height mode and the fluctuations in the current is monitored.

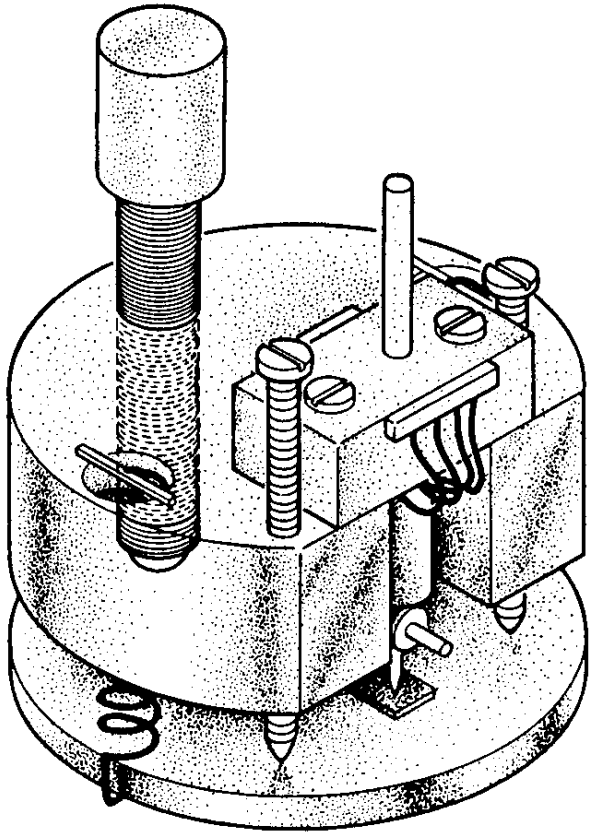

(b)

Imaging modes

1. Constant current
2. Constant height
3. dlnI/dz, modulating tip height and measuring current response one can get k or effective work function, ħ2k2/2m

FIG. 2.32 *(a) Simple schematic diagram showing the principal components of the scanning tunneling microscope. The emission tip or STM probe is positioned by piezodrives, P_z, P_x and P_y to map the speciman surface topography. (b) Schematic drawing of the STM (Courtesy John Clarke [64]. (c) SEM image of a tungsten STM probe tip being positioned over a graphite sample (Courtesy T. Hasegawa, Hitachi Central Research Laboratory), (d) Atomically resolved [111] silicon 7x7 structure [66].*

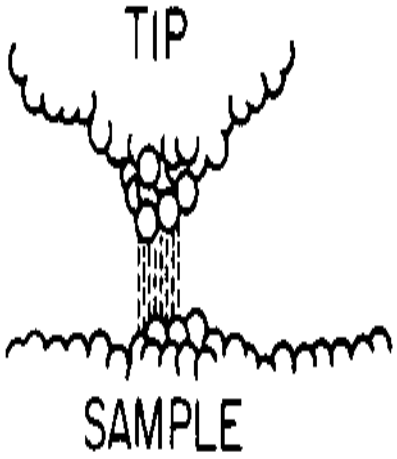

Even for a tip as large as a thousand atoms,
Only a few atoms take part in tunneling

FIG. 15. Naturally occurring protuberances reduce the area of the tunneling current, giving the STM its atomic resolution.

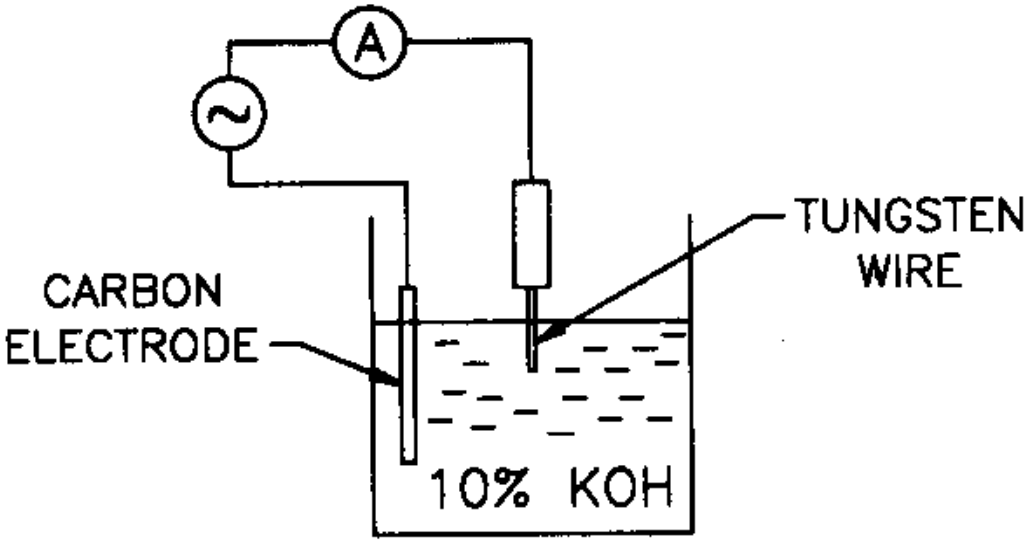

FIG. 16. Schematic drawing of an electrochemical tip-etching apparatus.

Components of an STM scanner

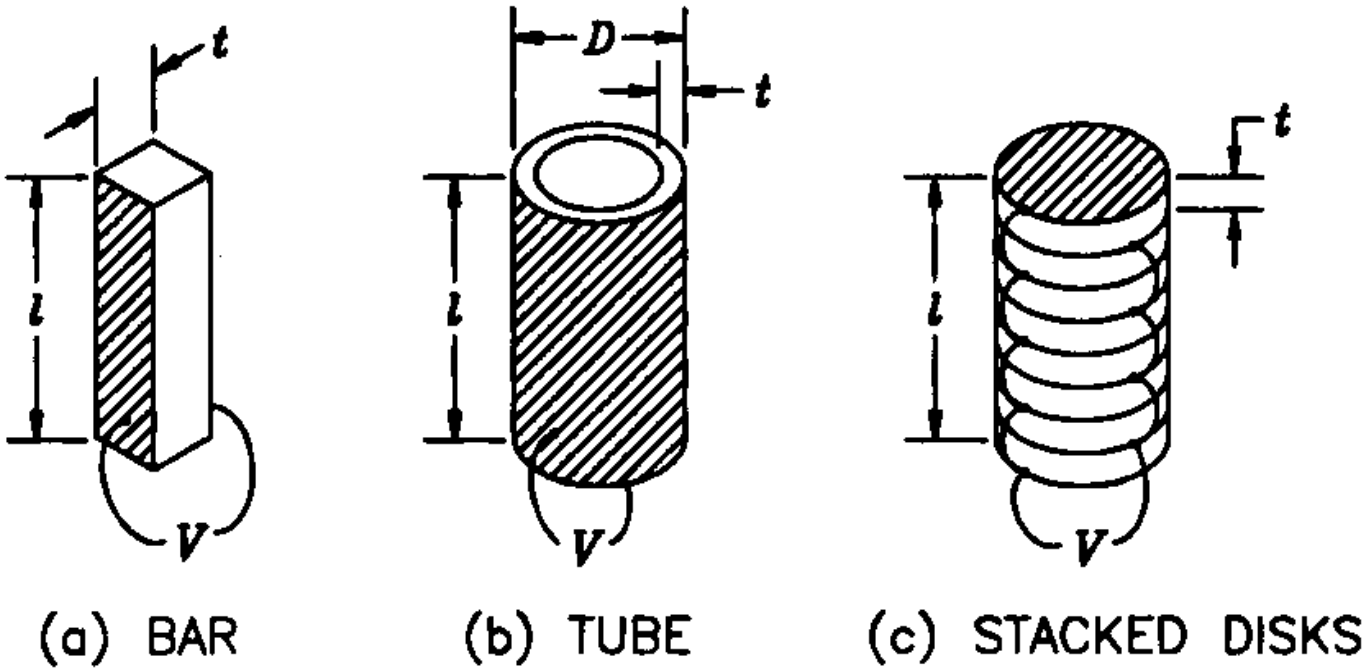

FIG. 17. Geometries of piezoelectric actuator elements.

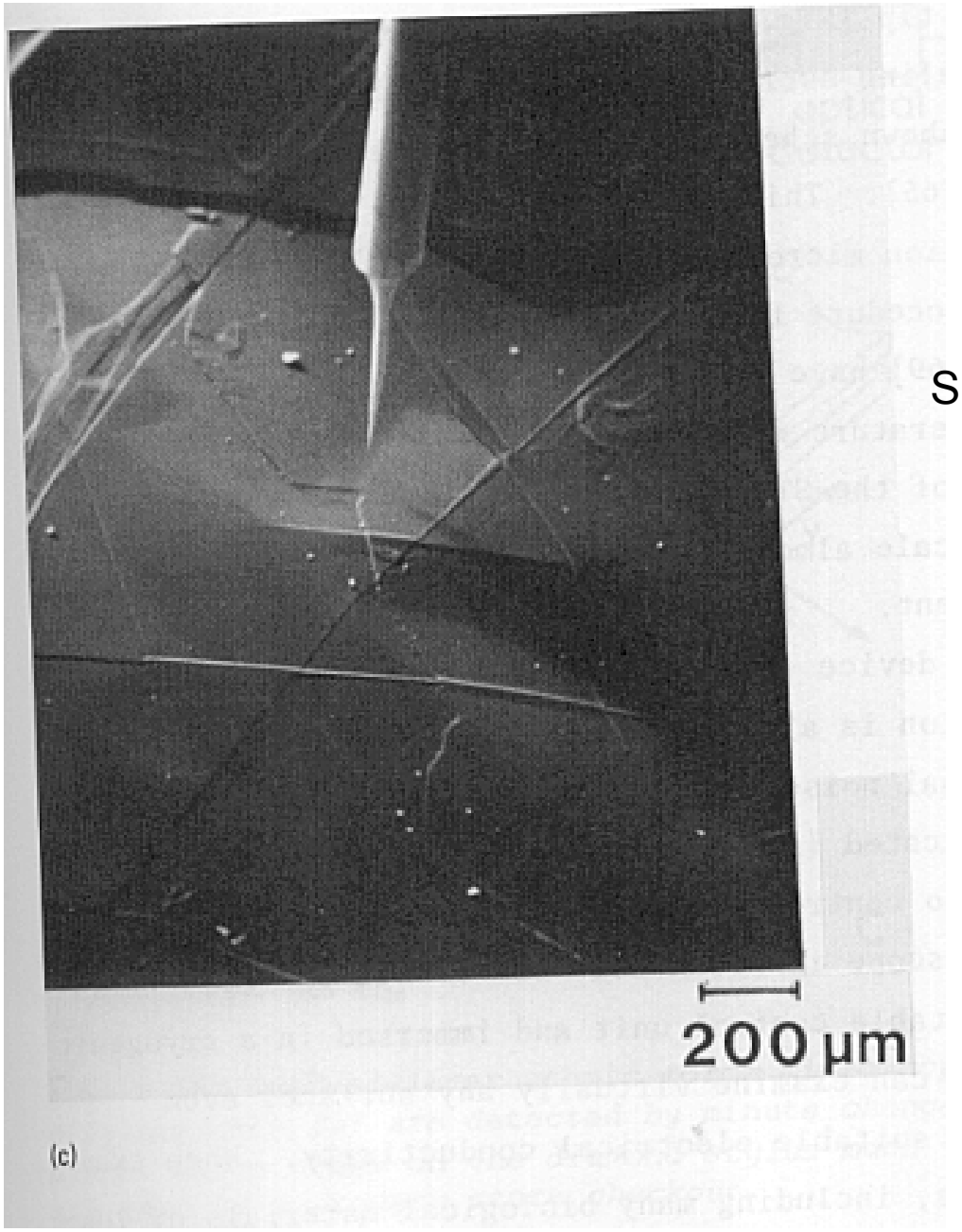

SEM image of a scanner

Applications
1. Surface structure

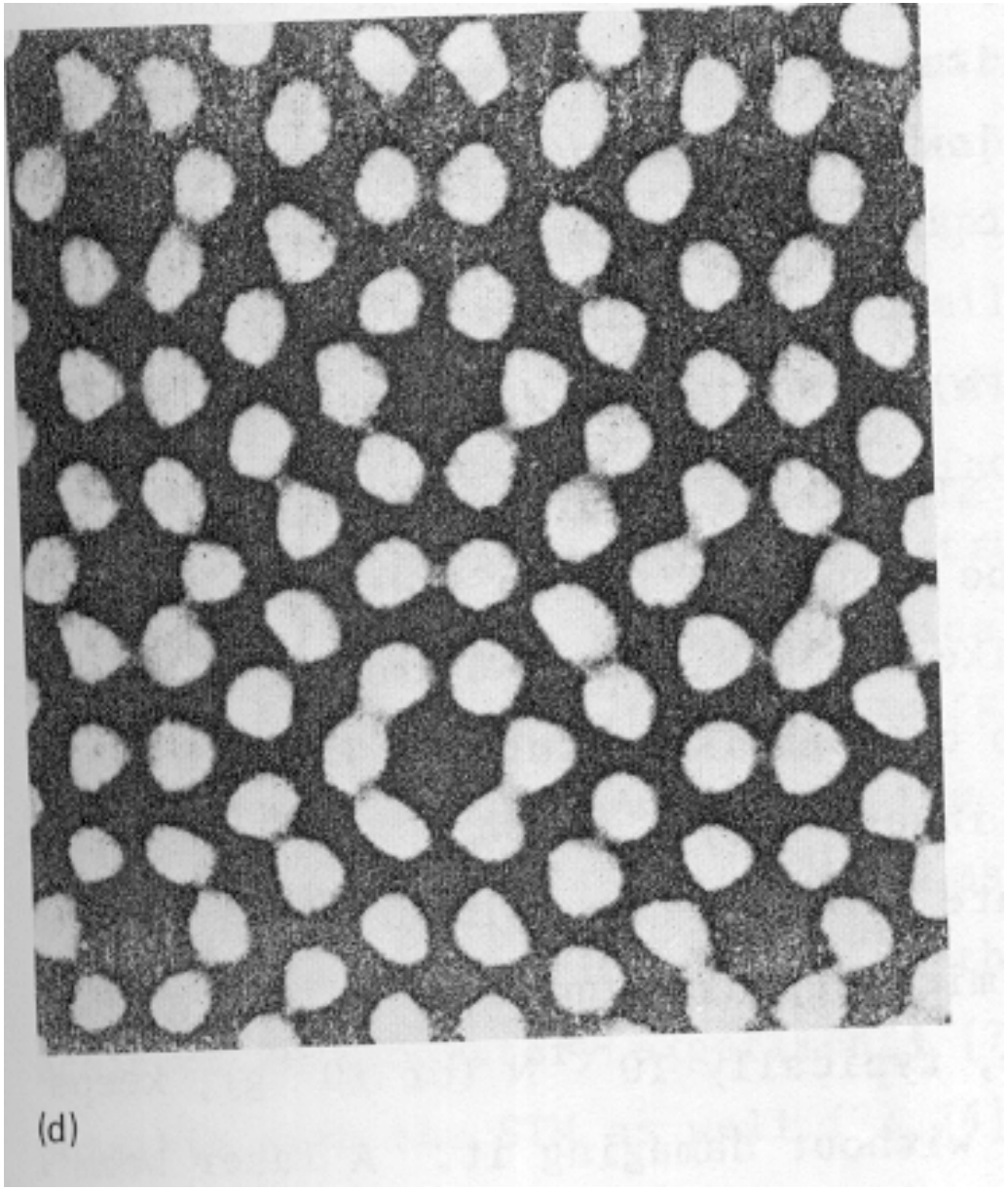

Si(7x7) surface, atomic resolution image

2. Density of states

This is evident in $\sqrt{E}$ dependence. CDW superstructure

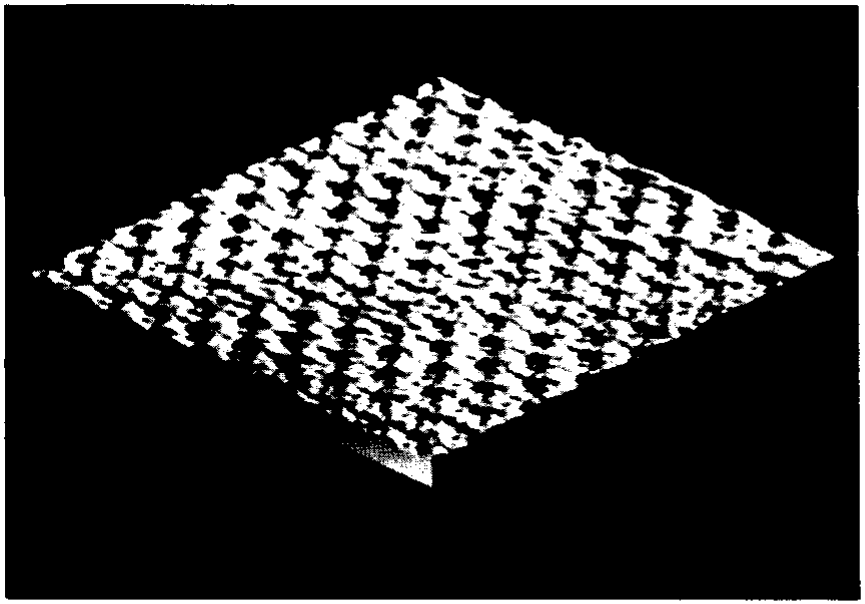

FIG. 2.34 *Local charge-density-wave (CDW) structure in 1T-TaS_2 single crystal surface determined by scanning tunneling microscopy. Courtesy John Clarke [64].*

3. Adsorbate structure (gold islands on graphite)

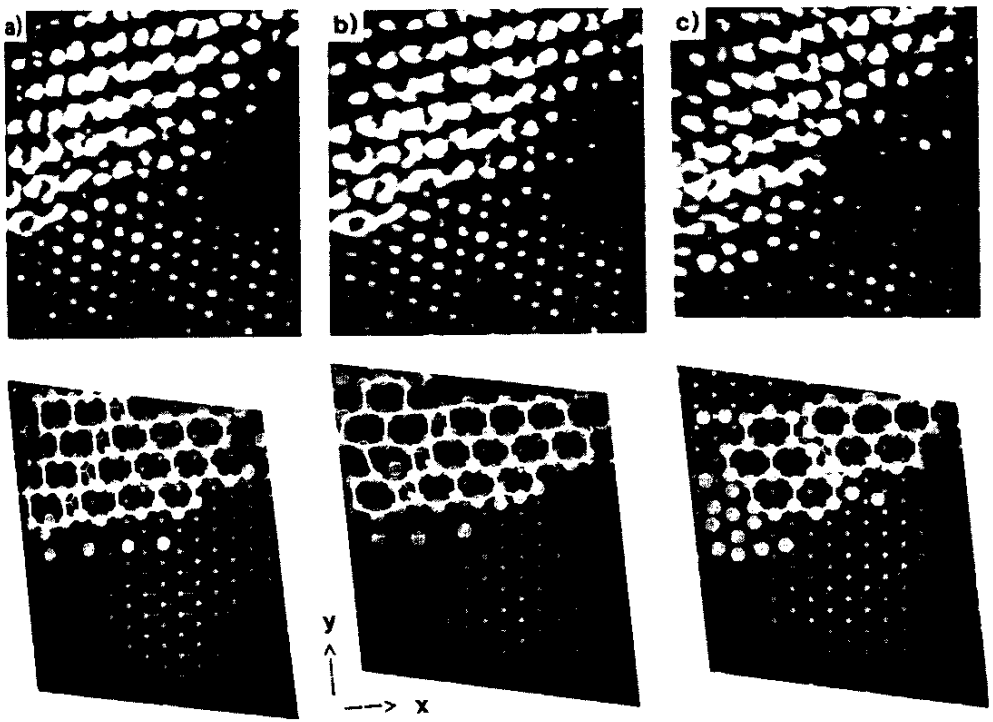

FIG. 2.35 *STM image of the local atomic structure of two-dimensional gold islands on graphite surface. Courtesy John Clarke [78].*

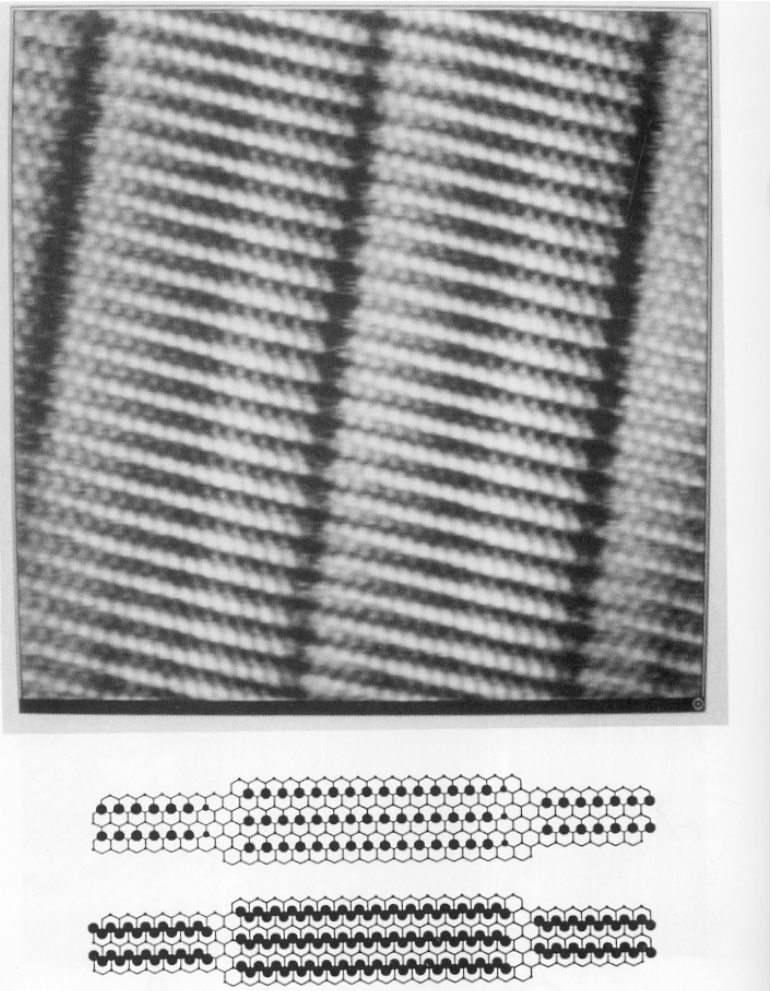

Plate 23. Organic molecules observed by STM. Upper, an STM image of n-$C_{32}H_{66}$ adsorbed on graphite. The length of these linear molecules is approximately 4 nm. Note the high degree of two-dimensional ordering; the long molecule axes are parallel, and troughs are formed where the ends of the molecules abut. The area is approximately 10×10 nm^2. Tip bias was 1 nA at 0.4 V (sample positive). Lower, a proposed model. (a) Graphite lattice with n-$C_{32}H_{66}$ molecules superimposed. (b) Careful observation of the angles and spacings in the STM image shows that its features correspond to those expected for graphite rather than n-$C_{32}H_{66}$ molecules. This implies an imaging mechanism whereby the tunneling sites inherent in the substrate are enhanced by the presence of the intermediate organic layer. See McGonigal, Bernhardt, and Thomson (1990) for details. Original image courtesy of D. J. Thomson.

4. Interfaces

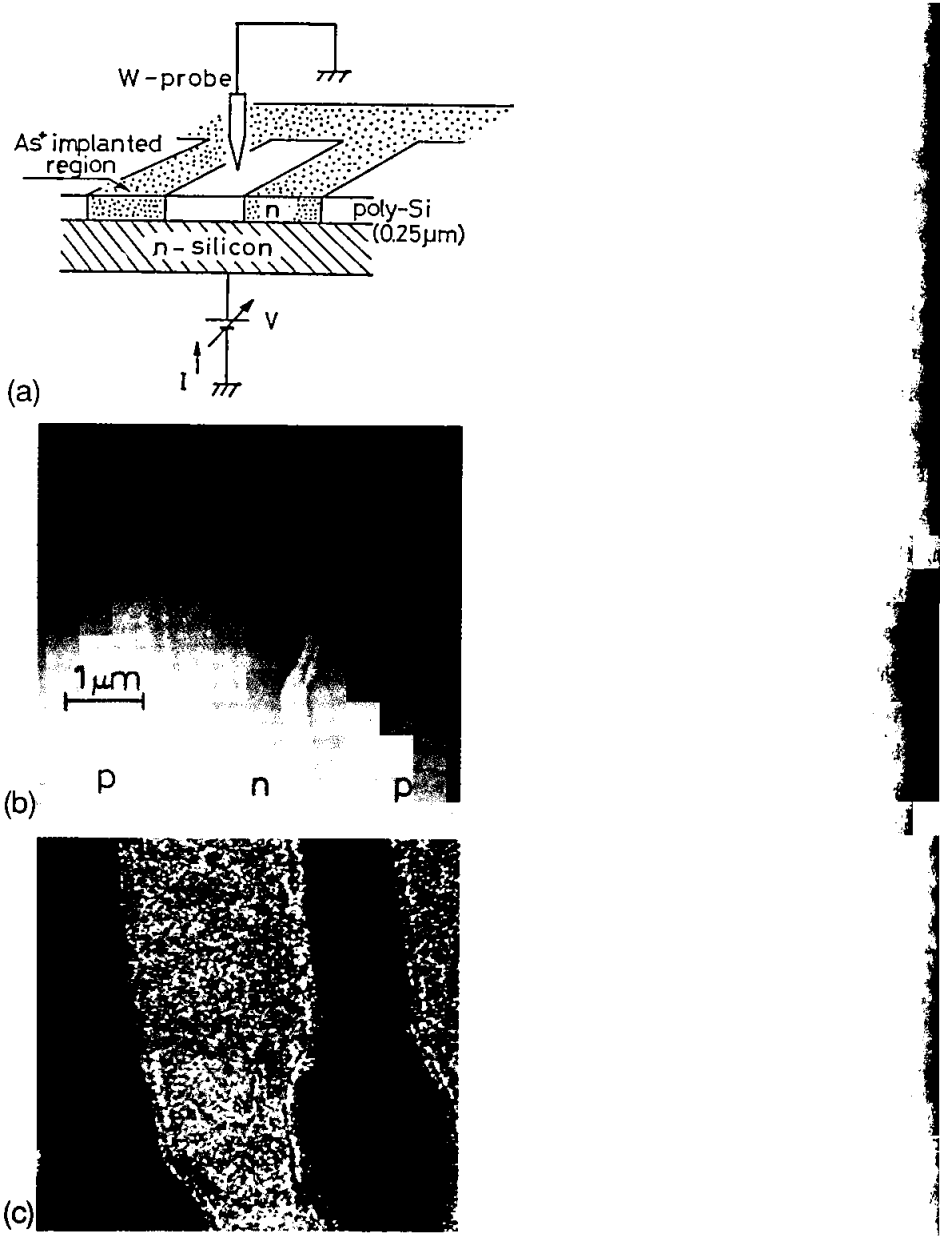

FIG. 2.36 *(a) Schematic diagram for STM imaging of Si pn junctions. (b) STM image of silicon surface with p and n-type areas at a tunnel (bias) voltage of -2.4 volts. (c) Same image area as (b) taken at +2 volts sample bias. Courtesy Dr. T. Hasegawa, Hitachi Central Research Laboratory [79].*

5. I vs. V measurement and its variations

Figure 41.4 Tunneling current–voltage (I–V) characteristic on clean UHV-cleaved p-type GaAs(110) surface. The bandgap (E_g), valence (V_b), and conduction (C_b) band onsets are shown.

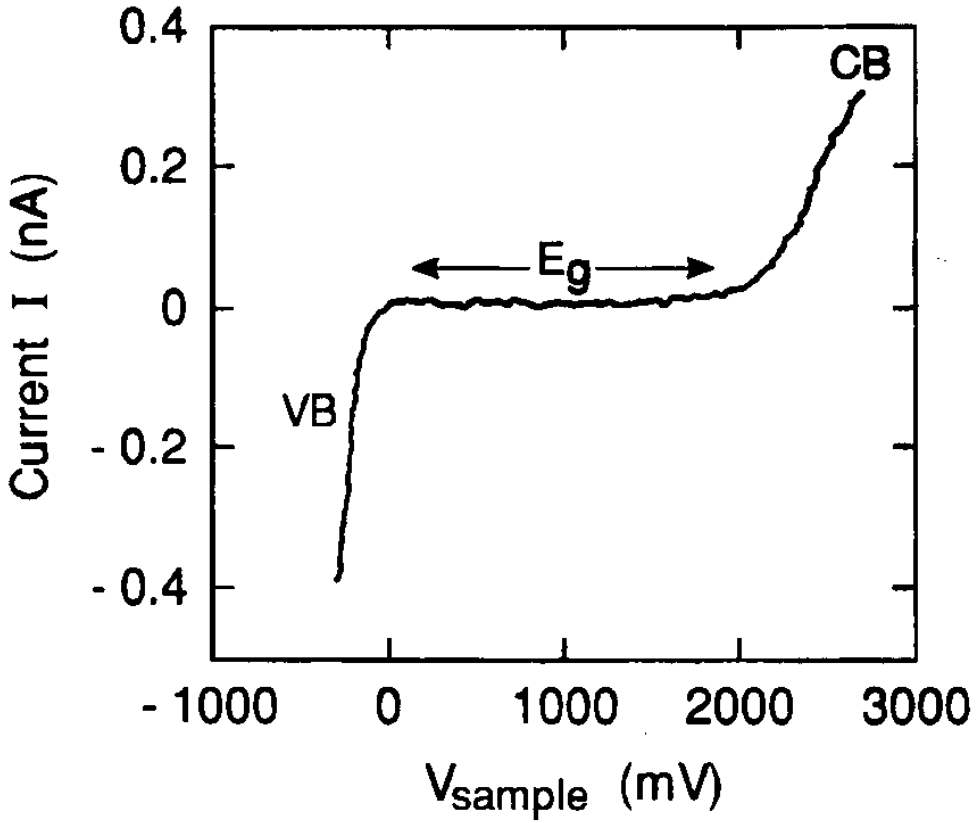

Various SXM techniques

TABLE I. SXM Techniques and Capabilities

1.	Scanning Tunneling Microscope (1981) —G. Binnig, H. Rohrer —Atomic resolution images of conducting surfaces
2.	Scanning Near-Field Optical Microscope (1982) —D. W. Pohl —50 nm (lateral resolution) optical images
3.	Scanning Capacitance Microscope (1984) —J. R. Matey, J. Blanc —500 nm (lat. res.) images of capacitance variation
4.	Scanning Thermal Microscope (1985) —C. C. Williams, H. K. Wickramasinghe —50 nm (lat. res.) thermal images
5.	Atomic Force Microscope (1986) —G. Binning, C. F. Quate, Ch. Gerber —Atomic resolution on conducting/nonconducting surfaces
6.	Scanning Attractive Force Microscope (1987) —Y. Martin, C. C. Williams, H. K. Wickramasinghe —5 nm (lat. res.) non-contact images of surfaces
7.	Magnetic Force Microscope (1987) —Y. Martin, H. K. Wickramasinghe —100 nm (lat. res.) images of magnetic bits/heads
8.	"Frictional" Force Microscope (1987) —C. M. Mate, G. M. McClelland, S. Chiang —Atomic-scale images of lateral ("frictional") forces
9.	Electrostatic Force Microscope (1987) —Y. Martin, D. W. Abraham, H. K. Wickramasinghe —Detection of charge as small as single electron
10.	Inelastic Tunneling Spectroscopy STM (1987) —D. P. E. Smith, D. Kirk, C. F. Quate —Phonon spectra of molecules in STM
11.	Laser Driven STM (1987) —L. Arnold, W. Krieger, H. Walther —Imaging by non linear mixing of optical waves in STM
12.	Ballistic Electron Emission Microscope (1988) —W. J. Kaiser (1988) —Probing of Schottky barriers on nm scale
13.	Inverse Photoemission Force Microscope (1988) —J. H. Coombs, J. K. Gimzewski, b. Reihl, J. K. Sass, R. R. Schlittler —Luminescence spectra on nm scale
14.	Near Field Acoustic Microscope (1989) —K. Takata, T. Hasegawa, S. Hosaka, S. Hosoki, T. Komoda —Low frequency acoustic measurements on 10 nm scale
15.	Scanning Noise Microscope (1989) —R. Moller, A. Esslinger, B. Koslowski —Tunneling microscopy with zero tip–sample bias

TABLE 1. Continued.

16.	Scanning Spin-precession Microscope (1989) —Y. Manassen, R. Hamers, J. Demuth, A. Castellano —1 nm (lat. res.) images of paramagnetic spins
17.	Scanning Ion-Conductance Microscope (1989) —P. Hansma, B. Drake, O. Marti, S. Gould, C. Prater —500 nm (lat. res.) images in electrolyte
18.	Scanning Electrochemical Microscope (1989) —O. E. Husser, D. H. Craston, A. J. Bard
19.	Absorption Microscope/Spectroscope (1989) —J. Weaver, H. K. Wickramasinghe —1 nm (lat. res.) absorption images/spectroscopy
20.	Phonon Absorption Microscope (1989) —H. K. Wickramasinghe, J. M. R. Weaver, C. C. Williams —Phonon absorption images with nm resolution
21.	Scanning Chemical Potential Microscope (1990) —C. C. Williams, H. K. Wickramasinghe —Atomic scale images of chemical potential variation
22.	Photovoltage STM (1990) —R. J. Hamers, K. Markert —Photovoltage images on nm scale
23.	Kelvin Probe Force Microscope (1991) —M. Nonnenmacher, M. P. O'Boyle, H. K. Wickramasinghe —Contact potential measurements on 10 nm scale

Atomic force microscopy

While STM is an electron microscope, AFM is a mechanical device. Here the mechanical motion of a tip is used to produce the image as illustrated. Just as in any mechanical instruments, AFM may be used to manipulate atoms and molecules at surfaces.

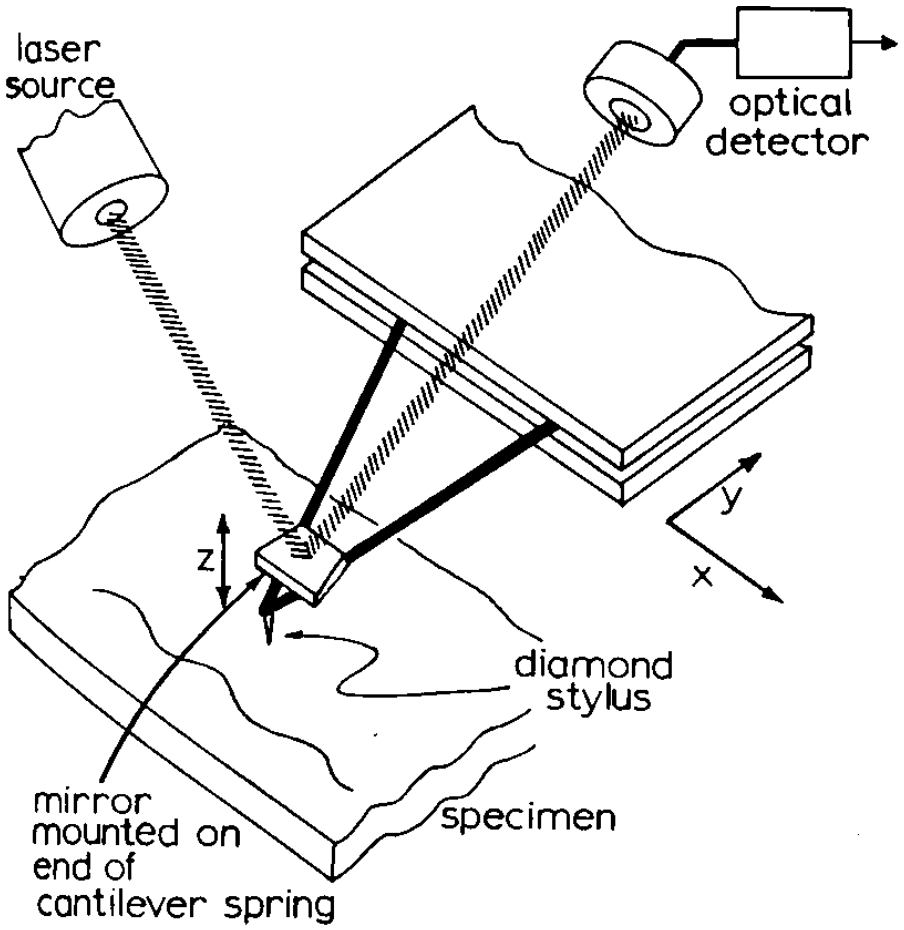

FIG. 2.33 *Optical-lever atomic force microscope schematic. Vertical displacements (z) are detected by minute changes in the position of the mirror which rides on the diamond stylus much the same way as bar codes are read in a grocery store checkout.*